ELSEVIER

Cement & Concrete Composites 22 (2000) 331–341

Cement & Concrete Composites

www.elsevier.com/locate/cemconcomp

A stereological approach to roughness of fracture surfaces and tortuosity of transport paths in concrete

Piet Stroeven *

Faculty of Civil Engineering and Geosciences, Delft University of Technology, Stevinweg 4, 2628 CN Delft, The Netherlands

Received 22 February 1999; accepted 27 April 2000

Abstract

Relatively weak interfaces between aggregate grains and the cementitious matrix initiate the damage evolution process leading to fracture. Coalescence between nearby interface cracks is promoted by the small nearest neighbour distances in a dense random packing of the aggregate. The fracture surface is therefore modelled as a dividing plane from which particles protrude. Assuming spherical aggregate, roughness is obtained as the global geometrical–statistical expression for the increase in fracture surface area due to a multitude of dome-like caps of various sizes. Transport phenomena in concrete are equally influenced by the aggregate, because traversing molecules or ions have to go around the dense grains. This route is additionally promoted by the relatively high porosity in the ITZ. Premature 'interface' cracking further reinforces this phenomenon. The planar and linear concepts of tortuosity in the transport path are analogous to those of roughness. Hence, the same estimates as developed for roughness will hold for tortuosity.

Keywords: Cementitious materials; Cracking; Diffusivity; Fracture surface; ITZ; Modelling; Particle–matrix interface; Particle size distribution; Roughness; Tortuosity

1. Introduction

Concrete is a macroscopically heterogeneous material. For design purposes this means that homogeneity can only be statistically defined for elements of macroscopical dimensions. Structure-sensitive mechanical properties (like cracking, or diffusivity) depend however on the structure of concrete inside this representative volume element (RVE). Concretes can be conceived on this level of the microstructure as a densely packed aggregate stabilised by a cementitious binder. The latter component constitutes the binding agent between the relatively dense, hard, stiff and strong multi-sized aggregate particles. Hereby, the particulate component is transformed into an effective load-bearing skeleton in the compression domain. The wider the range of particle sizes employed in the aggregate or in the (blended) cement, the higher the total packing density which can be achieved [1,2]. Yet, a finite pore space is always resulting, which should also be filled with the cementitious binder to prevent the ingress of harmful substances potentially endangering the integrity of the material body.

Under tensile loads, the skeleton cannot be effective, of course. Instead, it will be separated into portions by yielding of the bond between groups of particles and the cementitious binder. Globally speaking, this should occur in the weakest part of the body. However, macro-crack initiation takes place on meso- and even on microlevel. Complicated processes of micro-crack initiation and propagation, predominantly along the particle–matrix interfaces, will occur in scattered areas with a relatively unfavourable mix of residual and load-induced stresses and low strength capacity. This is accompanied by a process of redistribution of the load-induced stresses, whereby the afore-mentioned local mixes are changed. Upon load increase, larger cracks will be resulting from coalescence of interface cracks in areas where neighbouring micro-cracks happened to be on close distance and unfavouraby oriented with respect to the local principal tensile stress direction. This crack coalescence process will gradually concentrate in the so-called fracture process zone stretching over the full cross-section and with a thickness of only a very limited

* Tel.: +31-015-278-4035; fax: +31-015-261-1465.
E-mail address: p.stroeven@ct.tudelft.nl (P. Stroeven).

0958-9465/00/$ - see front matter
PII: S0958-9465(00)00018-4

number of times the maximum grain size. The interface cracks which will coalesce to form the macrocrack inside the fracture process zone will never be fully in-plane. However, the restricted extension of this zone in the loading direction will put a strict limit to the deviations of in-plane crack coalescence.

The body will be separated by way of the fracture surface in two parts. This fracture surface will bear evidence of the particulate nature of the material. An otherwise flat or slightly curved plane, the so-called dividing plane, reveals protruding particles that were in the path of the plane/crack. The morphological characteristics (texture) of the *fully developed* fracture surface can therefore be considered a 'fingerprint' of the material. Under compressive loads, generally, several fracture surfaces are formed, but the material's identity will be similarly reflected by the textural features of these fracture surfaces. *Roughness* is frequently employed to define surface texture in a global way (on the level of the RVE). The underlying crack deflection phenomenon governs material toughness [3], a mechanical property of considerable significance. This paper will not focus, however, on material behaviour. It will present an unbiased and objective way to quantitatively assess the morphological features of the material's fingerprint. This will allow to design and correctly evaluate experimentally, studies on mechanical properties such as strength, fracture toughness or fracture energy, that are at least partly governed by the morphological features of the fracture surface. Physico-mechanical models designed to predict material behaviour can also be provided with the relevant morphological information, when relevant.

Complete morphological characterisation of the afore-mentioned fingerprints of the material is a complicated task. In considering the material's strength and toughness, fracture surface roughness is a frequently used relevant aspect of this complete definition. This paper will as a consequence concentrate on this morphological feature of the fingerprints. However, it will also indicate other parameters for defining the 'uneveness' (i.e., the deviations from complete flatness) of the *fracture surface*.

A major external influence on roughness is exerted by the loading conditions. A 'fully developed' fracture surface can only arise under strain-controlled testing conditions. Under such conditions, the material will manifest post-peak strain softening behaviour. On structural level, cracks will be allowed to find the weakest link in the micro-mechanical system, i.e., the particle–matrix interfaces [4]. Otherwise, a fast growing crack will be formed which will cut its way through the particles, so that the fracture surface will degenerate into the dividing plane with a zero or at least dramatically reduced roughness.

Research has demonstrated the concept of a 'separation surface' between aggregate grains and the matrix in cementitious materials not to represent the actual transfer stage between the two components. In reality, a relatively thin interphase layer is formed around particles. This layer is generally attributed as Interfacial Transition Zone (ITZ). Micro-hardness measurements have indicated already quite some time ago the weakest area to be situated inside this layer [5]. Studies on particle packing in the ITZ by realistic computer simulations nowadays offer supporting evidence for these observations [6]. For estimation of *roughness* of a fracture surface, this would constitute a second-order effect, because for a very large majority of particles their sizes considerably exceed the ITZ's thickness. Hence, the thickness of the ITZ is taken zero in the model which will be developed for that purpose. The drop in hardness inside the ITZ is due to a relatively high internal porosity, which is confirmed by microscopical investigations [7]. This is a relevant phenomenon in durability studies in which the rate of ingress of gaseous or fluid substances into a concrete element is considered. A zero thickness of the ITZ is also assumed in the model which will be developed for estimating the *tortuosity* of the path ions or molecules have to follow through the concrete [8].

2. Morphological model

It is generally accepted for normal concretes, that cracks are readily initiated at particle–matrix interfaces at different levels of the microstructure under zero or relatively low loadings [9]. In a dense random packing of partly debonded aggregate particles, so typical for cementitious materials, the neighbouring bond cracks would be closely spaced [10]. This will easily give rise to crack coalescence among nearest neighbour pairs of cracks under relatively low loadings in the pre-peak range [11–13]. When only neighbouring pairs of bond cracks would coalesce along a common dividing plane, this would already lead to a considerable amount of structural disintegration, as visulalized in Fig. 1 [13]. Deformation-controlled experiments in the direct compression and tension domains revealed crack extension data of the same order of magnitute at ultimate [4]. Hence, a major part of the *crack concentration process* in (or close by) the dividing plane takes place in the post-peak region inside the narrow fracture process zone. This reduces the chances for uncontrolled cracking in a direction deviating significantly from the dividing plane.

The simplest morphological concept which can be derived from the foregoing is sketched in Fig. 2 [14]. It is similar to the model underlying the transport problem. The otherwise flat plane of progress of an echelon of

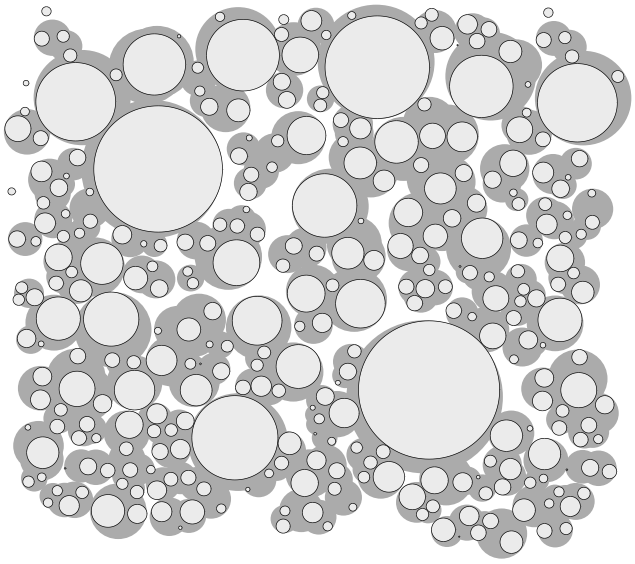

Fig. 1. Crack extension in a dividing plane by coalecence of neigbouring pairs of bond cracks.

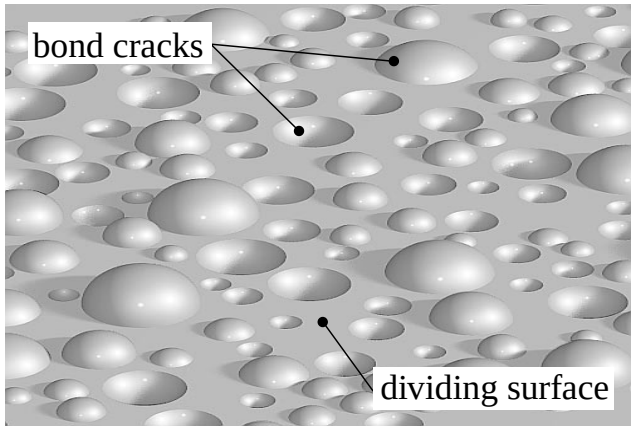

Fig. 2. Computer-simulated surface composed of inter-connected planar portions of a dividing plane (DP) and protruding dome-like caps of spherical aggregate particles.

ions or molecules is bent around particle obstacles. The model concept shows a surface of macroscopical dimensions (at least corresponding to those of the RVE). It is composed of inter-connected planar parts of a dividing plane, and of dome-like caps and indentations of spherical particles intersecting with the plane. Because of obvious reasons, the largest part of each particle is embedded. Fig. 3 presents a blown up part of Fig. 2, revealing a single particle cap protruding from the dividing (or cross-sectional) plane. In transport or fracture problems alike, the textural finger print originating from the large number of caps and indentations should be quantified. For that purpose, the contribution to these textural features of an arbitrary particle cap as shown in

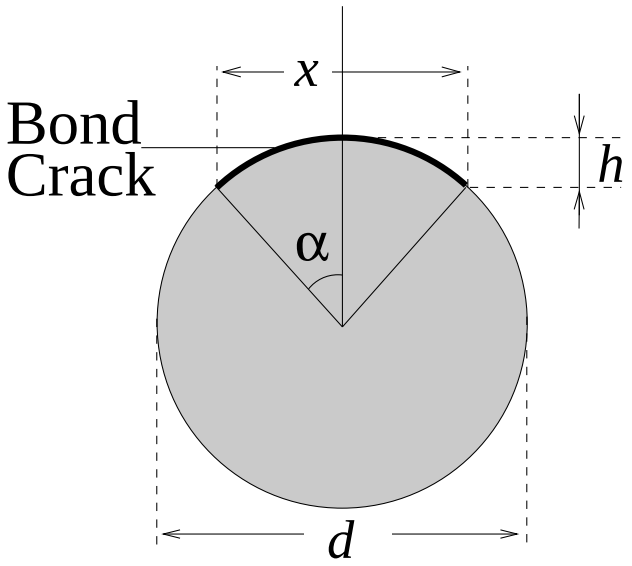

Fig. 3. Geometry of the cap of a particle intersecting a dividing plane (DP).

Fig. 3 should be elaborated first. Global measures of texture can be obtained by averaging over all caps in the dividing plane. Roughness is only one of such possible measures. The morphological model, though simple, offers a fairly good textural approximation for the fracture surface or the transport path in cementitious materials, provided the boundary conditions are fulfilled (hard spherical aggregate grains, a relatively weak and porous ITZ, deformation-controlled test conditions). If so, the morphology should be characterized in an objective and unbiased way, to provide relevant structural information for physico-mechanical models of material behaviour, or to allow proper structural interpretation of experimental data pertaining to such properties.

3. Texture analysis – mono-sized aggregate

The diameter of the intersection circle and the height of the cap are denoted by x and h, respectively, as shown in Fig. 3. The solution to the morphological problem is governed by the size distribution functions of x and h, defined by $\Phi(x)$ and $\Psi(h)$, respectively.

$\Psi(h)$ is readily obtained. All values of h between 0 and $d/2$ are equally likely. Here, d is particle diameter. Hence,

$$\Psi(h) = 2/d. \tag{1}$$

The first and second moment are respectively ($d =$ constant)

$$\overline{h} = \frac{2}{d}\int_0^{d/2} h\,\mathrm{d}h = \frac{d}{4}, \tag{2}$$

$$\overline{h^2} = \frac{2}{d}\int_0^{d/2} h^2\,\mathrm{d}h = \frac{d^2}{12}, \tag{3}$$

$\Phi(x)$ is governed by an integral equation of Abel's type [9,15]

$$\Phi(x) = \frac{x}{\overline{d}}\int_x^{d_m} \frac{f(d)}{\sqrt{d^2 - x^2}}\,\mathrm{d}d \tag{4}$$

in which $\overline{d}$ and d_m are the average and largest observed particles in the aggregate. $f(d)$ is the particle size distribution (psd) function.

For mono-sized spheres, Eq. (9) reduces to [9,14]

$$\Phi(x) = \frac{x}{d\sqrt{d^2 - x^2}}. \tag{5}$$

The literature offers a direct relationship between the moment generation functions of x and d, however, which simplifies the calculation of the moments of $\Phi(x)$. The derivation is presented in [9].

$$m_n(x) = M_n(d)\int_0^{\pi/2} (\sin\phi)^{n+1}\,\mathrm{d}\phi \tag{6}$$

in which n indicates the number of the moment and $m_n(x)$ and $M_n(d)$ denote the moment generating functions of x and d, respectively. For mono-sized spheres it is found that

$$\begin{aligned} m_1(x) &= \frac{\pi}{4}M_1(d) = \frac{\pi}{4}d, \\ m_2(x) &= \frac{2}{3}M_2(d) = \frac{2}{3}d^2. \end{aligned} \tag{7}$$

The surface area of a dome-like cap of a sphere is given by [14]

$$S = \pi\left(h^2 + \frac{1}{4}x^2\right). \tag{8}$$

Hence, the average surface area of all caps amounts

$$\overline{S} = \pi\left(\overline{h^2} + \frac{1}{4}\overline{x^2}\right) = \frac{\pi}{4}d^2. \tag{9}$$

The number of caps is N, and the area of the dividing plane A. The density of caps in this plane is therefore $N/A = N_A$. Since, $N_A = dN_V$, with N_V as the spatial density of particles, it is found that

$$N_A = d\frac{V_V}{(\pi/6)d^3} = \frac{6V_V}{\pi d^2}. \tag{10}$$

The total surface area per unit of the dividing plane, S_A is found upon combining Eqs. (9) and (10)

$$S_A = \overline{S}\cdot N_A = \frac{3}{2}V_V, \tag{11}$$

V_V in the last two relationships denotes the volume fraction of the observed aggregate. S_A, i.e., the relative extent of the ITZ in the fracture or transport surface, does not depend on particle diameter, and will as a consequence for a multi-sized particle distribution not depend on the size distribution function (sieve curve).

4. Single cap morphology – multi-sized aggregate

For multi-sized aggregates, the derivation follows similar lines. It has been shown earlier [14], that for continuously graded mixes where the sieve curves fall inside the practical area indicated in building codes, the psd can generally be formulated by

$$f(d) = q\frac{d_0^q}{d^{q+1}}, \tag{12}$$

where d_0 defines the smallest particles in the aggregate observed in an experimental approach, or included in a model for estimating purposes. d_0 therefore defines the *sensitivity* of the concept. Only for a (very) high sensitivity level, whereby all particles in the aggregate are involved, d_0 can be associated with the smallest particles in the aggregate. A mono-sized aggregate will result at the lowest possible sensitivity level.

For $q = 2.5$ or $q = 3$ in Eq. (12), a so-called Fuller mix or an equal volume fractions mix are obtained. Their psd's are respectively

$$f(d)_{\mathrm{FM}} = \frac{5}{2}\frac{d_0^{2.5}}{d^{3.5}}, \tag{13}$$

$$f(d)_{\mathrm{EV}} = 3\frac{d_0^3}{d^4}. \tag{14}$$

The moment generation function of Eq. (12) is

$$M_n(d) = \overline{d^n} = \int_{d_0}^{d_m} d^n f(d)\,\mathrm{d}d. \tag{15}$$

Table 1 lists the moments for $n = 1, 2$ and 3 for the psd's of Eqs. (13) and (14). It can be seen that the equal volume fractions mix (EV) has the smallest average

Table 1
Moments of the psd's corresponding to the boundaries of the sieve curves prescribed by the building code[a]

	$\overline{d}$	$\overline{d^2}$	$\overline{d^3}$	$\overline{d_c}$	$\overline{d_c^2}$
$f(d)_{\mathrm{FD}} = (5/2)d_0^{2.5}/d^{3.5}$	$(5/3)d_0$	$5d_0^2$	$5d_0^{2.5}d_m^{0.5}$	$3d_0$	$3d_0^{1.5}d_m^{0.5}$
$f(d)_{\mathrm{EV}} = 3d_0^3/d^4$	$(3/2)d_0$	$3d_0^2$	$3d_0^3\ln(d_m/d_0)$	$2d_0$	$2d_0^2\ln(d_m/d_0)$

[a] Herein d_0 and d_m are the smallest, respectively largest particles in the model; d_c is the size of a particle intersecting a plane.

grain size of the two. This points toward the larger number of smaller particles in this mix. This is visualised in Fig. 4, revealing sections of concretes, containing aggregates based on the respective sieve curves, and compacted to maximum density (generated by SPACE system).

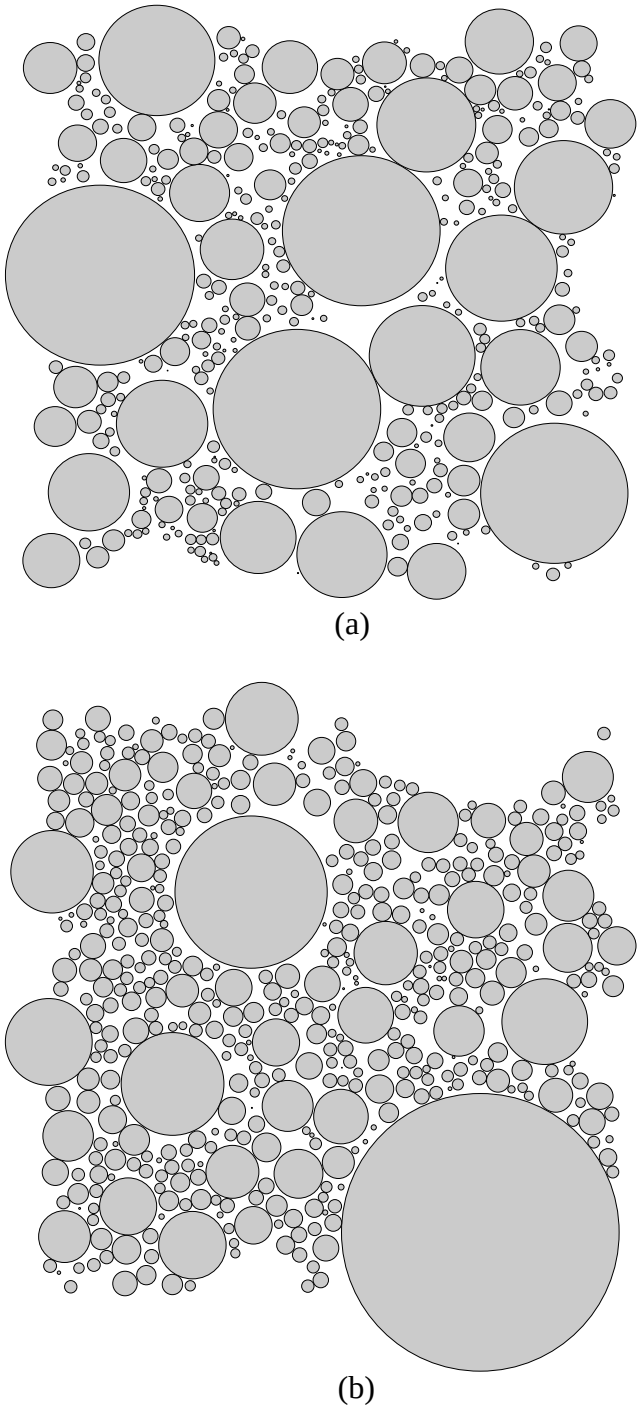

Fig. 4. Sections through computer-generated aggregates compacted to maximum density based on a Fuller (a) and an equal volume fraction sieve curve (b); results were obtained by SPACE system [9].

For completeness sake and to prevent misinterpretations, the parameter $\overline{d}_c$ is added in Table 1. $\overline{d}_c$ is the average size of only those grains which intersect a random plane, or in the present case, the dividing plane. These particles govern the texture of the fracture surface or the transport path of traversing ions or molecules. A comparison with $\overline{d}$ demonstrates that a section plane, crack plane or dividing plane yields *biased* information on the psd in *bulk*, hence on the bulk composition (grading) of the aggregate. This can simply be accounted for by adding to the psd in bulk the relative probability that a (random, crack or dividing) plane intersects with an arbitrary particle, i.e., $d/\overline{d}$. Popularly speaking, smaller particles are easily missed by cutting the specimen. Hence, the two psd's for only the particles intersecting the dividing, crack or cross-sectional plane are

$$g(d_c)_{FM} = \frac{d_c}{\overline{d}} f(d_c)_{FM} = \frac{3}{2}\frac{d_0^{1.5}}{d_c^{2.5}}, \tag{16}$$

$$g(d_c)_{EV} = \frac{d_c}{\overline{d}} f(d_c)_{EV} = 2\frac{d_0^2}{d_c^3}. \tag{17}$$

The moments in Table 1 can readily be obtained from these psd's. They reveal the relative 'coarsening' of the particle mixture governing texture, as compared to the grain mixture used to make the concrete.

5. Texture analysis – multi-sized aggregate

To determine $\overline{S}$ according to (9), the second moments of h and x should be available. Thereupon, the cap density, N_A, should be assessed on the basis of moments of the psd, which are given in Table 1. Eqs. (1) and (6) are used for the determination of $\overline{h^2}$ and $\overline{x^2}$. The results for the two different sieve curves are collected in Table 2. For comparison reasons, also the psd's according to Eqs. (16) and (17) are elaborated and plotted in the last column. These psd's could be derived from quantitative section analysis, but they would *incorrectly* represent bulk features.

Application of Eq. (9) yields the values of average cap surface area. Results are given in Table 3. The number of caps per unit of the plane, N_A, is obtained in analogy with Eq. (10) from

$$N_A = \frac{6}{\pi}\frac{V_V}{\overline{d^2}}. \tag{18}$$

For the two sieve curves this yields for the bulk case

$$N_A(\mathrm{FM}) = \frac{6}{5\pi}\frac{V_V}{d_0^2}, \tag{19}$$

$$N_A(\mathrm{EV}) = \frac{2}{\pi}\frac{V_V}{d_0^2}. \tag{20}$$

It is obvious from Tables 2 and 3, that for both sieve curves the value of S_A is given by

Table 2
Moments of height, h, and span, x, of particle caps protruding from the dividing or cross-sectional plane, in which the psd's are associated with Fuller and constant volume fraction mixes[a]

Type of sieve curve	Parameter	Aggregate in bulk	Aggregate in plane
Fuller	$\overline{h}$	$(5/12)d_0$	$(3/4)d_0$
	$\overline{h^2}$	$(5/12)d_0^2$	$(1/4)d_0^{1.5}d_m^{0.5}$
	–	–	–
	$\overline{x}$	$(5\pi\ /12)d_0$	$(3\pi\ /4)d_0$
	$\overline{x^2}$	$(10/3)d_0^2$	$2d_0^{1.5}d_m^{0.5}$
Equal volume fraction	$\overline{h}$	$(3/8)d_0$	$(1/2)d_0$
	$\overline{h^2}$	$(1/4)d_0^2$	$(1/6)d_0^2\ln(d_m/d_0)$
	–	–	–
	$\overline{x}$	$(3\pi\ /8)d_0$	$(\pi/2)d_0$
	$\overline{x^2}$	$2d_0^2$	$(4/3)d_0^2\ln(d_m/d_0)$

[a] At the left, all particles in bulk contribute to the psd, at the right, the psd is solely based on the particles intersecting the dividing or cross-sectional plane.

Table 3
Average surface area, $\overline{S}$, of caps of aggregate particles protruding from the dividing or cross-sectional plane[a]

Type of sieve curve	Parameter	Aggregate in bulk	Aggregate in plane
Fuller	$\overline{S}$	$(5\pi\ /4)d_0^2$	$(3\pi\ /4)d_0^{1.5}d_m^{0.5}$
Equal volume fraction	$\overline{S}$	$(3\pi\ /4)d_0^2$	$(\pi/2)d_0^2\ln(d_m/d_0)$

[a] Data are based on the moments of psd's given in Table 2.

$$\overline{S}N_A = S_A = \frac{3}{2}V_V \tag{21}$$

as was also derived for the mono-sized case (Eq. (11)). Hence, the result is *not depending on the details of the actual sieve curve*. Eq. (21) is valid for a random distribution of aggregate particles. Violating this condition by aligning all relevant particles with their centres in the dividing plane (a very unlikely situation), would bring the constant in Eq. (21) to 2, which can be considered the upper bound value.

The global expressions on $\overline{h}$, $\overline{h^2}$ and S_A reflect various measures for the uneveness of a fracture surface or transport path. Either one of such measures can be employed in physico-mechanical models for specific characteristic material properties. The choice depends on the property to be modelled, and the degree of sophistication of the model. On the one end of the range, $\overline{h}$ is simply a one-dimensional measure equal to the average amplitude of the uneveness. S_A, at the other end of the range, is a two-dimensional measure dealing with the relative extent of the surface area contributing to the uneveness. This range of measures for uneveness can be enlarged [16]. For example, $\overline{h^2}$ could be multiplied by the frequency of the uneveness, per unit of area: N_A. This leads to $\overline{h^2}N_A = V_V/2\pi$. In analogy, $\overline{h}$ could be multiplied by $\sqrt{N_A}$, leading to a one-dimensional measure for roughness, that is proportional to $\sqrt{V_V}$. The constant in the equation is different, however, for the various sieve curves (because $\overline{d}/\sqrt{\overline{d^2}}$ is depending on the psd). For shear fracture, the so-called *particle interlock mechanism* should be modelled. The resistance to in-plane deformations is conventionally related in such an approach to the in-plane and the out-of-plane projected areas of the caps, per unit area of the dividing plane [17,18]. The second is easily obtained, i.e., $A_{A\perp} = \pi\overline{x^2}N_A/8 = V_V/2$. The first is given by (see Fig. 3) $A_{A\parallel} = \overline{d^2}(\overline{2\alpha} - \overline{\sin 2\alpha})N_A/8 = 3(1-4/\pi^2)V_V/8$. Substitution in the expressions for $\overline{h}$, and $\overline{h^2}$ of the appropriate moments of d given in Table 1 will finally yield various measures for uneveness, some of which are independent from the details of the sieve curve (S_A, $\overline{A}_{A\perp}$ and $\overline{A}_{A\parallel}$, as well as $\overline{h^2}N_A$), whereas others depend on such details ($\overline{h}$, $\overline{h^2}$, and $\overline{h}\sqrt{N_A}$).

6. Roughness and tortuosity

The planar index of surface roughness or tortuosity, R_s, is defined as the ratio of total surface area and the corresponding (projected) area of the dividing plane. The linear roughness index is analogously defined. A so-called vertical section (i.e., perpendicular to the dividing plane) delineates a profile in the surface which is subjected to texture analysis. The linear roughness index

equals the ratio of the length of the profile and the corresponding (projected) length in the divided plane. The situations are sketched in Fig. 5. Hence, the planar values of *roughness* and of *tortuosity* are given by

$$R_s = A_{Am} + S_A = 1 + S_A - V_V = 1 + \frac{1}{2}V_V \tag{22}$$

in which A_{Am} represents the areal fraction of the matrix along the divided plane, and $S_A = (3/2)V_V$. Obviously, roughness and tortuosity do not depend on the size distribution of the spheres, and hence not on the details of the sieve curve.

Basically, this holds only for a 2-D (=planar) portion of cracks 'parallel' to the dividing plane. Similar remarks can be made as to the route molecules and ions follow through the concrete. When a significant portion of interfaces tends to be debonded in the virgin state, this 'random' phenomenon will exert an influence on crack coalescence and crack concentration processes, and thus on roughness (and tortuosity). Hence, for a proper assessment of such texture parameters, it could be necessary to also consider a 3-D random portion of bond cracks in the vicinity of the dividing plane. This leads to the concept of a partially-planar system of dispersed caps that should be described [13].

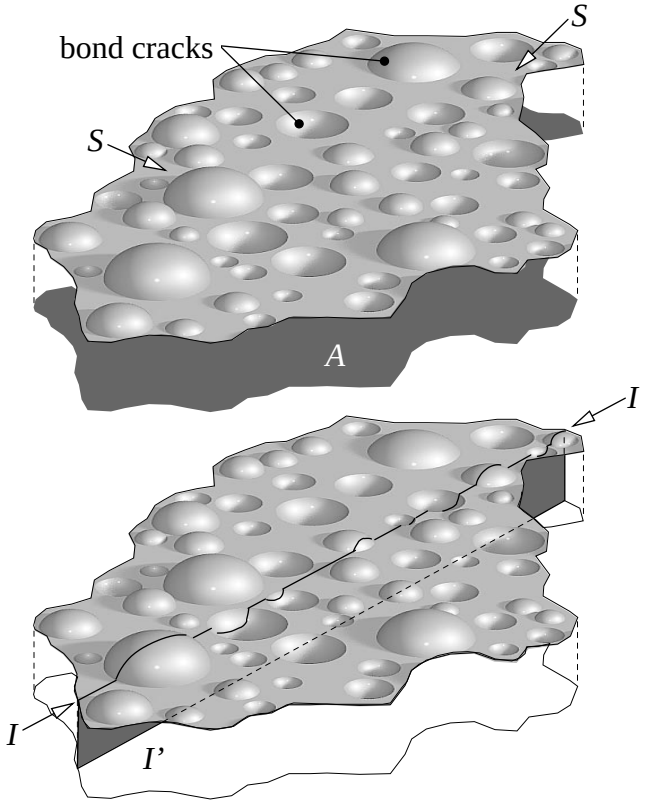

Fig. 5. Definitions of planar roughness index, $R_s = S/A$, and linear roughness index, $R_l = l/l'$.

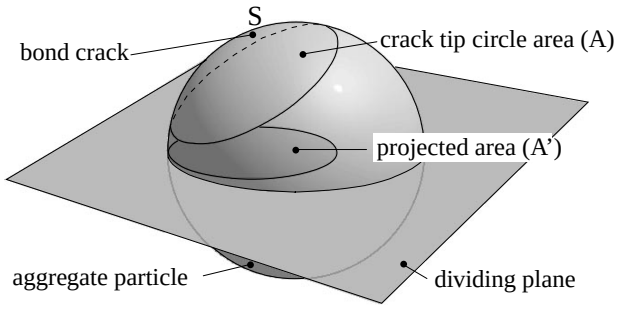

Fig. 6. Geometry of a bond crack in a 3-D system with respect to the dividing plane.

The problem is solved in two successive steps. In the first, the ratio is determined of the average surface area of the caps, $\overline{S}$, and the average area enclosed by the circular crack tip region, $\overline{A}_c$. As in the 2-D case, this amounts to $3/2(=\overline{S}/\overline{A}_c)$, provided bond crack extension is assumed similar as in the 2-D case. This seems a rough approximation, but the 3-D contribution to roughness and tortuosity is in general probably quite small. In the second step, these randomly distributed 'circular crack tip regions' are projected on the nearby dividing plane. The average projected area, $\overline{A'}$, is half as large as the original one $(\overline{A}_c/\overline{A'} = 2)$. Combination of the two steps yields $S_{A'} = 3(=\overline{S}/\overline{A'})$. This situation is sketched in Fig. 6. Hence, Eq. (22) can be modified to encompass both the 2-D and 3-D portions,

$$\begin{aligned} R_s &= 1 - V_V + 3V_{V3} + \frac{3}{2}V_{V2} \\ &= 1 + 2V_V\left(1 - \frac{3}{4}\omega\right) \quad \left(\omega = \frac{V_{V2}}{V_V}\right), \end{aligned} \tag{23}$$

where the indices 2 and 3 refer to the 2-D and 3-D portions, respectively. The solution for planar tortuosity is identical. For $\omega = 1$, Eq. (22) is regained. The linear roughness index, R_l can be approximated for the present purpose by $R_l \approx 1 + \pi(R_S - 1)/4$ [19]. Substitution of Eq. (23) leads to

$$R_l \approx 1 + \frac{\pi}{2}V_V\left(1 - \frac{3}{4}\omega\right). \tag{24}$$

The linear tortuosity index is also given by Eq. (24)

7. Profile measurements

For modelling purposes, the planar concept should be selected, because of the physical similarity with the actual situation. This holds for fractographical as well as transport problems. However, when it is experimentally pursued to measure profiles of fracture surfaces or potential transport routes, the linear concept would offer the correct and more handy analytical framework. The

sensitivity of the experiments and of the analytical model *should be attuned to each other*. This basically governs the assessment of the lower threshold value, d_0, provided this exceeds the size of the smallest particles in the material system (concrete or mortar aggregate, cement grains, silica fume). Hence, this implies the sole factor to govern roughness or tortuosity, i.e., volume fraction of aggregate, also to depend on the sensitivity level. When a comparative study is made into the effect of only the coarse aggregate on permeability, V_V in Eqs. (21)–(24) denotes the volume fraction of only the coarse aggregate [9].

When simplifying assumptions as to the grain shape seem unrealistic, or when it is pursued because of other reasons to experimentally assess roughness or tortuosity indices, the profile length, l, can easily be determined using stereological approaches. Linear roughness and tortuosity are defined by

$$R_l = \frac{l}{l'}, \tag{25}$$

where l' is the total projection of l on the dividing or cross-sectional plane. l' can be determined in an unbiased way by measuring its total projected length in a number of randomly selected directions, and averaging of the outcomes. Thus,

$$l = \frac{\pi}{2}\overline{l'}. \tag{26}$$

For completeness sake, it can be mentioned here that the method can also be extended to cover a (large) number of lines in a plane, such as a network of crack traces in a section plane [20].

Determination of the profile length can also be accomplished without making measurements at all. Instead, the method of random or directed secants is employed. To do so, the profile is enclosed by a square frame with area, A. Next, a line grid is superimposed in an arbitrary direction defined by an angle θ. The following equality holds:

$$P_L(\theta) = l'_A\left(\theta + \frac{\pi}{2}\right). \tag{27}$$

Although this equality is attributed to Cauchy, it was applied for the present purpose by Steinhaus in 1930 (see, [15]). Hence, the number of intersections with the (fracture) profile, P, per unit of the grid line length inside the frame, L (i.e., P_L), in a direction θ equals (in probability terms) the total projection, l', of the profile in an orthogonal direction (i.e. $\theta + (\pi/2)$), per unit of the frame area, A. So, instead of *measuring* total projected length in n directions, the number of intersections between a sweeping test line system and the profile is *counted* in a similar number of directions. The accuracy of the sample average is high; the ratio of the sample average and the population value will be situated between $\pi\cos(\pi/2n)(2n\sin(\pi/2n))^{-1}$ and $\pi(2n\sin(\pi/2n))^{-1}$ [8,15], where $2n$ denotes the number of equally spaced directions of sampling between 0 and 2π.

It should be noted that for the *present model* the linear roughness or tortuosity index can be assessed in an objective and unbiased way as well, hence avoiding the approximation involved in Eq. (24). In [21] it is shown that ($\omega = 1$, for simplicity reasons)

$$R_l = 1 + V_V\left(\frac{\pi^2}{8} - 1\right). \tag{28}$$

By combining Eqs. (11) and (28), it is seen that $R_s \approx 2R_l - 1$, which is basically only valid for the concept of a fracture plane (or transport path) composed of a flat dividing plane and protruding spherical particles. Coster and Chermant [22] developed an expression for a more general concept that is only restricted by upper bounds for R_l and R_s (irrelevant in case of concrete). The given expression is: $R_s = 2(R_l - 1)/(\pi - 2) + 1$. This expression is identical to the one developed in this paper for $\pi = 3$, generalising the validity of this equation relating R_l and R_s. Hence, even in an experimental approach where the grain shape would deviate (considerably) from the spherical one, the planar roughness index could be estimated by this equation, after determination of the profile roughness by the sweeping test line approach.

8. Discussion

The developed analytical system for modelling morphological parameters, such as in the present case tortuosity and roughness, has been successfully applied to estimate fractal properties of the fracture surface and of damage evolution stages in concrete [23,24]. This is possible because 'roughness' is presented as a function of sensitivity, M ($M = d_{max}/d_0$). Hence, using Eq. (28), $R_l \approx 1 + 0.25V_V(M)$. The sieve curves lead to near self-similarity situations with respect to the texture of the fracture surface at different resolution levels (but within the size range of the aggregate, of course). The resolution-dependence can thus be expressed by means of the fractal equation

$$\log R_l = (D_l - 1)\log M + C, \tag{29}$$

D_l is the fractal profile dimension and C a constant (determination of which can be avoided by considering the slope of the curves). Solutions have been determined for different sieve curves in a limited range of sieve fractions, assuming $\omega = 1$ in Eq. (23), yielding fractal dimensions around 1.15, which is close to *experimentally obtained* data available in the literature [25]. In the relevant tests, a large concrete block was separated in two parts by splitting action. The fracture surface could be

modelled by only assuming 2-D in-plane coalesced microcracks. When a deformation-controlled test is conducted on a small-scale concrete specimen, the roughness of the fracture surface will increase due to out-of-plane microcrack formation. This can be incorporated in the ω-value. In general, Eq. (29) will depict slightly curved lines for different sieve curves of continuously graded aggregate mixtures, revealing the non-ideal fractal properties of the fracture surface within the size range of the aggregate. Similar remarks can be made as to the transport case, where tortuosity can also be interpreted in terms of its non-ideal fractal nature. High density concretes reveal an increased brittleness. As a result, cleavage of particles will be more dominant, reducing roughness and as a consequence also fractal dimension of the fracture surfaces. This has been *experimentally confirmed* [26].

For $V_V = 0.5$, Eq. (28) yields a value of 1.125. This is on the regression line of volume fraction versus tortuosity data, presented in [8]. Volume fraction was *experimentally obtained* and tortuosity was determined by *computer-simulation*. This linear dependence is in accordance with the analytical solution presented in this paper. The regression line in [8] can only be considered a rough approximation of the data, however, due to the significant amount of scatter (see [8, Figs. 13 or 16]). Hence, the analytical expressions are preferable, because they are exact and readily available, so do not need time-consuming simulation work. Although outside the scope of this paper, the experimental data on *physico-mechanical behaviour* on artificial concretes presented in [8] confirm the dominant influence of roughness and tortuosity. Major care should therefore be bestowed on properly defining/determining this parameter, which was the prime goal of this publication.

Use of this analytical concept would have (partly) changed the interpretation of the experimental data. The coalescence of neighbouring interfacial bond cracks (or the transport through the matrix) is supposed to take place along the dividing plane (or parallel to it on a relatively short distance). The distance between neighbouring aggregate particles in *normal* concrete is very small. Average nearest neighbour distance in the dividing plane between the fully developed interface cracks (or the ITZ's), $\overline{\Delta}_2$, would be [9]: $\overline{\Delta}_2 = 0.5/\sqrt{N_A}$ (valid for cracks/ITZ's 'randomly' distributed in the dividing plane). Upon substitution of Eq. (18), the expression is transformed into: $\overline{\Delta}_2 = 0.63\sqrt{\overline{d^2}/V_V}$. This leads to values of $\overline{\Delta}_2$ only slightly exceeding *minimum* grain size (depending on M, and on the sieve curve). The same holds for $\bar{x}$. Since average free spacing equals the difference between these values, this confirms that the path length through the matrix will be on average very small, indeed. Of course, deviations from randomness might cause the 0.5 factor in the first expression for the average nearest neighbour distance to somewhat increase, but this will not affect the conclusion drawn on small inter-crack spacing in the dividing plane. This can be visualised by adding still finer particle fractions to Fig. 1. Each particle fraction reduces the displayed distances in proportion to the added particle size. Since size is on a logarithmic scale, distances will decline sharply in this process. These very small distances are a prerequisite for the mechanism of prevailed crack coalescence or transport through the matrix. This condition is not fulfilled for the artificial concretes investigated in [8].

Upon improvement of the relevant ITZ properties with respect to those of the matrix (i.e., strength, porosity), crack coalescence or transport routes might start deviating from the afore-mentioned concept, because a short-cut between neighbouring ITZ's, somewhat away from the dividing plane, will become preferable because of energy considerations. This would set a limit to the *relevance of the morphological model* used in this paper for the unbiased and objective assessment of a measure for tortuosity and roughness. Still, the presented solutions would offer the main influence, so that the intensity of short-cutting could be assessed in this way.

S_A in Eq. (11) is an unbiased and objective measure for the relative planar extent of the ITZ (in the surface under consideration). Since a one-to-one relationship exists between tortuosity (or roughness) and the extent of the ITZ (it can readily be seen from Eqs. (11) and (22) that $S_A = 3(R_s - 1)$), it could be expected that the *experimental data* in [8] will also reveal this linear dependence of the ITZ's extent on volume fraction, and they do indeed. For additional experimental use of the roughness and tortuosity concept in experiments (again, not targeted in this paper), see the relevant literature (e.g., a series of references is provided in [8]).

Since tortuosity would be still proportional to the volume fraction of aggregate particles up to maximum density, and the total volume fraction of the aggregate is restricted by physical conditions, the suggestion of a "threshold aggregate content, above which the transport should increase drastically" [7] does not seem realistic, and is not supported by experimental evidence either (as indicated in [7]).

The ITZ in the present context of this paper is seen as a packing discontinuity at the surface of aggregate particles. This discontinuity is studied by SPACE in [6,27]. Results generally confirm the concluding remarks by Bentur at the end of a recent International Conference on the Interfacial Transition Zone [28]. As a *systems parameter*, the packing characteristics reflect the compositional features of the material (i.e., the psd of the cement, addition of mineral admixtures, water to binder ratio) and the production technology. Discontinuities near interfaces in particle density or particle grading were found significantly different in these

simulated concretes. This inevitably leads to different measures for the extent of the ITZ. After hydration, the porosity, among other things, is still found affected by the packing discontinuity. Generally speaking, porosity was found higher in the ITZ than in bulk for normal concretes (for conventionally applied water to cement ratios). This would also lead to locally reduced strength properties. These two ITZ characteristics were on the basis of the concept for roughness and tortuosity developed in this paper.

9. Conclusions

A method is described based on geometrical probability theory, that provides objective and unbiased measures for *fracture surface roughness*, or for the *tortuosity of transport routes* in cementitious materials. The underlying morphological model conceives the material as composed of a dense random packing of a multi-sized spherical aggregate and a uniform cementitious matrix. The bond between hard and dense aggregate grains and the matrix is supposed to be the weakest micromechanical link. Similarly, the water-born ions and molecules that will traverse the material body are supposedly forced to go around these grains. The latter phenomenon will be stimulated in practice by a relatively thin but porous ITZ. The morphological model is therefore in both cases a (flat) dividing plane and dome-like caps of the spherical particles intersecting this plane.

Mechanical or physical properties of cementitious materials, such as strength, fracture toughness, fracture energy, diffusivity or conductivity, will be (partly) governed by the grain-induced uneveness of this fracture or transport surface. The literature provides some supporting experimental evidence for these dependences. The described solutions make it possible to quantitatively evaluate such experiments in terms of the major parameters governing the investigated behaviour. Constitutive modelling for describing the physico-mechanical behaviour of cementitious materials in the afore-mentioned areas, should be based on a correct dependence of behaviour on relevant structural features, such as roughness and tortuosity, as provided in this paper.

Additionally, this paper provides other practical measures for defining the uneveness of the fracture or transport surface, such as the average amplitude, or cap height, $\overline{h}$, and its two-dimensional analogue, $\overline{h^2}$, and the orthogonal components of the projected areas of the caps, $A_{A\perp}$ and $A_{A\parallel}$. The latter two measures are employed in shear strength modelling. Finally, the frequency of the uneveness of the surface under consideration is introduced, by multiplication of the one-dimensional measure $\overline{h}$ by $\sqrt{N_A}$, and the two-dimensional measure $\overline{h^2}$ by N_A. This leads to a series of alternative measures which are all independent from the details of the sieve curve, i.e., S_A, $\overline{h^2}N_A$, $A_{A\perp}$ and $A_{A\parallel}$.

Since measurements can more easily be performed on profiles, also the linear concept of roughness and tortuosity is in use. These solutions are therefore also presented. Further, the method of total projections is introduced as an accurate and unbiased way to measure the profile length. Alternatively, an approach by a sweeping test line is proposed to reduce the effort to counting only.

The analytical measures for linear or planar roughness and tortuosity are demonstrated not to depend on the details of the sieve curve. The effect of the extent of the ITZ on diffusifity, referred to in some experimental studies, is shown to be directly correlated to the tortuosity effect. Hence, only a single *morphological* parameter, i.e., volume fraction, should be distinguised in experimental evaluation or constitutive modelling approaches. Details of the sieve curve will exert influences on behaviour because of other operating mechanisms. In Fig. 4 two section images are displayed of computer-simulated concretes with identical maximum volume density of 0.74. The applied aggregate mixtures are close to the respective limits of the sieve curve area in building codes. The section patterns are quite distinct, reflecting the differences in the fineness modulus of the aggregate, being 5.9 and 7.3, respectively. Producing concretes with such different mixtures will cause the ITZ's to have different physico-mechanical properties, that influence observed behaviour. But in both cases, roughness or tortuosity are identical. A marginal effect might only be due to different short-cut tendencies.

References

[1] Jiang W, Roy DM. Strengthening mechanisms of high-performance concrete. In: Malhotra VM, editor. High Performance Concrete, Proc ACI Int Conf Singapore. Detroit: ACI, 1994. p. 753–67.

[2] Fidjestøl P, Frearson J. High performance concrete using blended and triple blended cements. In: Malhotra VM, editor. High Performance Concrete, Detroit: ACI, 1994. p. 135–57.

[3] Abell AB, Lange DA. The role of crack deflection in toughening of cement-based material. In: Brandt AM, Li VC, Marshall IH, editors. Brittle matrix composites, vol. 5. Cambridge: Woodhead, 1997. p. 241–50.

[4] Stroeven P. Some observations on microcracking in concrete subjected to various loading regimes. Engrg. Fract. Mech. 1990;35(4/5):775–82.

[5] Lyubimova TY, Pinus ER. Crystallization structure in the contact zone between aggregate and cement in concrete. Colloid J. USSR 1962;24(5):491–8.

[6] Stroeven P, Stroeven M. Micromechanical behaviour of concrete interpreted by computer simulation systems for material structure. In: Carlomagno GM, Brebbia CA, editors. Computational methods and experimental measurements IX. Southampton: WIT Press, 1999. p. 571–82.

[7] Diamond S, Huang J. The interfacial transition zone: realityor myth? In: Katz A, Bentur A, Alexander M, Arliguie G, editors. Interfacial transition zone in cementitious composites. London: E & FN Spon, 1998. p. 3–39.
[8] Jaiswal SS, Igusa T, Styer T, Karr A, Shah SP. Influence of microstructure and fracture on the transport properties in cement-based materials. In: Brandt AM, Li VC, Marshall IH, editors. Brittle matrix composites, vol. 5. Cambridge: Woodhead, 1997. p. 199–220.
[9] Stroeven P. Some aspects of the micro-mechanics of concrete, Ph.D. thesis. Delft: Delft University of Technology, 1973.
[10] Stroeven M, Stroeven P. Simulation of hydration and the formation of microstructure. In: Owen DRJ, Oñate E, Hinton E, editors. Computational plasticity. Barcelona: CIMNE, 1997b. p. 981–87.
[11] Nied HA, Arin K. Multiple flaw fracture mechanics model for ceramics. In: Bradt RC, Hasselman DPH, Lange FF, editors. Fracture mechanics of ceramics, flaws and testing, vol. 3. New York: Plenum Press, 1978. p. 67–83.
[12] Koiter WT. An infinite row of collinear cracks in an infinite elastic sheet. Ingenieur Arch. 1959;28:168–72.
[13] Stroeven P. Study of crack development as the basis for rheology of cementitious materials. In: Wang R, editor. Proc IUTAM Symp Rheology of Bodies with Defects, Dordrecht: Kluwer Academic Publishers, 1999. p. 205–22.
[14] Stroeven P. Structural modelling of plain and fibre reinforced concrete. J. Comp. 1982;April: 129–39.
[15] Kendall MG, Moran PAP, Geometrical probability. London: Griffin, 1963.
[16] El-Soudani SM. Profilometric analysis of fractures. Metallography 1979;11:247–336.
[17] Stroeven P, Stroeven M. Microstructural modelling of shear resistance of cracked concrete. In: Owen DRJ, Onate E, Hinton E, editors. Computational plasticity, fundamentals and applications, Barcelona, Spain: CIMNE, 1997. p. 1568–73.
[18] Walraven JC. Aggregate interlock: a theoretical and an experimental analysis, PhD thesis. Delft: Delft University of Technology, 1980.
[19] Underwood EE. Stereological analysis of fracture roughness parameters. Acta Stereol. 1987;6(Suppl II): 170–78.
[20] Ringot E. Automatic quantification of microcracks network by stereolgical method of total projections in mortars and concretes. Cement Concrete Res 1988;18:35–43.
[21] Stroeven P. Stereological estimates for roughness and tortuosity in cementitious composites. Proc X ICS, 1–4 November. Australia: Melbourne, 1999 [to be published in special issue of Acta Stereologica, 2000].
[22] Coster M, Chermant JL. Recent developments in quantitative fractography. Int. Metals Rev. 1983;28(4):228–50.
[23] Stroeven P. Fractals and fractography in concrete technology. In: Brandt AM, Marshall IH, editors. Brittle matrix composites, vol. 3. London: Elsevier Applied. Science, 1991. p. 1–10.
[24] Stroeven P. Stereological estimation of fractal number of fracture planes in concrete. In: Cummins HZ, Durian DJ, Johnson DL, Stanley HE, editors. Disordered materials and interfaces, MRS 407. Pittsburgh, 1996. p. 343–48.
[25] El-Saouma VE, Barton CC. Fractal characterization of fracture surfaces in concrete. In: Gamaleldin NA, editor. Engrg. Frac. Mech. 1990;35-1: 47–53.
[26] Rawicki Z, Wojnar L. On quantitative fractographic analysis of high density concretes. Acta Stereol. 1992;11/2:185–9.
[27] Stroeven M. Discrete numerical modelling of composite materials; application to cementitious materials, PhD thesis. Delft: Delft University of Technology, 1999.
[28] Bentur A. ITZ structure and its influence on engineering and transport properties: concluding remarks to the conference. In: Katz A, Bentur A, Alexander M, Arliguie G, editors. Interfacial transition zone in cementitious composites. London: E & FN Spon, 1998. p. 335–37.